Theory on Capillary Filling of Polymer Melts in Nanopores

Yang Yao,[1] Hans-Jürgen Butt,[1] George Floudas,[1,2] Jiajia Zhou,[3,4,*] and Masao Doi[4]

[1] *Max Planck Institute for Polymer Research, D55128 Mainz, Germany*

[2] *Department of Physics, University of Ioannina, P.O. Box 1186, 451 10 Ioannina, Greece*

[3] *Key Laboratory of Bio-Inspired Smart Interfacial Science and Technology of Ministry of Education, School of Chemistry, Beihang University, Beijing 100191, China*

[4] *Center of Soft Matter Physics and Its Applications, Beihang University, Beijing 100191, China*

(Dated: January 30, 2018)

Abstract

We present a unified theory for the imbibition dynamics of entangled polymer melts into nanopores. Experiments [J. Chem. Phys. **146**, 203320 (2017)] demonstrated the validity of $t^{1/2}$ dependence but contradicted the predictions of the classical Lucas-Washburn equation because of the prefactor. A reversal in dynamics of capillary filling has been reported with increasing polymer molecular weight. Polymer imbibition under nanometer confinement can be discussed by two mechanisms: One is the standard hydrodynamic flow, resulting in a parabolic flow profile. When the inner wall has a strong attraction to the polymer, a layer of immobile chains is created, resulting in an increase of the effective viscosity and to slower imbibition. The other is the reptation model proposed by Johner et al. [Europhys. Lett. **91**, 38002 (2010)], leading to a plug flow profile and to the reduction in the effective viscosity (faster imbibition). The reversal in dynamics of polymer imbibition can be explained by the competition between these two mechanisms.

* jjzhou@buaa.edu.cn

1. INTRODUCTION

Understanding fluid dynamics in a confined geometry is important in many different fields such as engineering, physics, chemistry, biotechnology, and nanotechnology. Successful applications include the development of inkjet printheads for commercial xerography, synthesis and production of various nanoparticles and polymeric materials on a lab-on-a-chip device, separation and manipulation of DNA or other biomacromolecules, and on-the-spot medical diagnosis in clinical pathology. Under spatial confinement, the volume of the fluid reduces, and the surface-to-volume ratio increases. This leads to the fact that the interaction between the fluid and the surface, i.e., the capillary effect, becomes the dominant factor among many other interactions. A canonical example is the fluid imbibition into a pore with hydrophilic inner surfaces. For Newtonian fluid, the standard model to describe the imbibition dynamics is the celebrated Lucas-Washburn equation (LWE) [1, 2]

$$h(t) = A\, t^{1/2}, \quad A = \sqrt{\frac{R\gamma \cos\theta_{\mathrm{E}}}{2\eta_0}} \tag{1}$$

Here $h(t)$ is the imbibition length of the fluid inside the pore, R is the pore radius, γ is the surface tension of the fluid, θ_{E} is the equilibrium contact angle, and η_0 is the fluid viscosity in the bulk. The dynamical scaling of $t^{1/2}$ has been found in many phenomena involving capillarity and wetting [3]. Extensive studies by experiments [4–7], theory [8, 9], and simulations [10–12] have advanced our understanding on the capillary filling, but there are still new avenues to be explored [13, 14].

An implicit assumption in the derivation of Lucas-Washburn equation is that the size of fluid particles should be an order of magnitude smaller than the pore radius. This is valid for simple fluids, for example, when water (10^{-10} m) fills a μm-size glass pore. Experimentalists nowadays can probe the range where the two length scales are comparable: for example, when a polymer (radius of gyration $R_g \sim 10 - 100$ nm) penetrate into self-ordered nanoporous aluminum oxide (AAO) (also $R \sim 10 - 100$ nm) [13, 14]. Surprisingly, the dynamical scaling of $t^{1/2}$ is consistently observed in experiments and remains valid in the nanometer ranges. However, the prefactor A exhibits interesting behaviors even for simple liquids [5].

From the experimentally measured A value, one can deduce an effective viscosity

$$\eta_{\rm eff} = \frac{R\gamma\cos\theta_{\rm E}}{2A^2}. \tag{2}$$

The value of $\eta_{\rm eff}$ is in general different than the bulk value η_0.

Recent experiments have shown a complex behavior of the effective viscosity for capillary imbibition of polymer melts into nanoscale pores [14]. Capillary penetration of a series of entangled poly(ethylene oxide) (PEO) melts within nanopores of self-ordered alumina followed $h \sim t^{1/2}$ behavior according to the LWE. However, a reversal in dynamics of capillary filling has been observed with increasing polymer molecular weight. Polymer chains with 50 entanglements or less showed a slower capillary filling than theoretically predicted, indicating a higher effective viscosity. For longer chains with more entanglements, the capillary filling was faster than the theory and the effective viscosity was reduced as compared to bulk. In this paper, we present a possible explanation for this unusual observation.

2. THEORETICAL CONSIDERATIONS

We first present a brief derivation of the Lucas-Washburn equation. Let us consider a cylindrical pore of radius R (schematically shown in Fig. 1). One end of the pore is in contact with a Newtonian fluid bath, and the fluid is drawn into the pore under capillarity. The dynamics of the filling can be described by $h(t)$, the length of the fluid inside the pore.

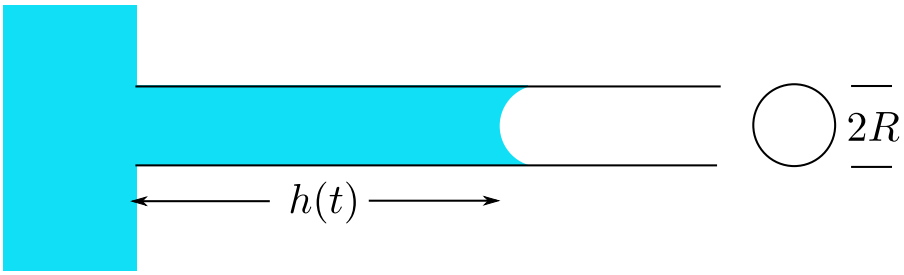

FIG. 1. A sketch of fluid imbibition into a cylindrical pore.

There are two opposite forces acting on the fluid.

(i) Capillary force

$$F_{\rm c} = 2\pi R(\gamma_{\rm SV} - \gamma_{\rm SL}) = 2\pi R\gamma\cos\theta_{\rm E}, \tag{3}$$

where $\gamma_{\rm SV}$, $\gamma_{\rm SL}$ and γ are the interfacial tension between solid/vapor, solid/fluid, and fluid/vapor, respectively. These three interfacial tensions are related by the Young's relation, $\gamma_{\rm SV} - \gamma_{\rm SL} = \gamma \cos\theta_{\rm E}$, where $\theta_{\rm E}$ is the equilibrium contract angle. Here we only consider a hydrophilic surface, i.e., $\theta_{\rm E} < 90°$. The capillary force drives the imbibition.

(ii) Viscous force

$$F_{\rm v} = 8\pi\eta_0 h v, \tag{4}$$

where η_0 is the fluid's viscosity and $v = {\rm d}h/{\rm d}t$ is the filling speed. The prefactor depends on the pore geometry, and for circular pore it equals to 8π. The viscous force provides the friction against the imbibition.

The balance between the capillary and viscous forces results in the evolution equation

$$2\pi R\gamma\cos\theta_{\rm E} = 8\pi\eta_0 h v \tag{5}$$

$$\Rightarrow \quad v = \frac{R\gamma\cos\theta_{\rm E}}{4\eta_0 h}. \tag{6}$$

The solution to the above equation is

$$h^2 = \frac{R\gamma\cos\theta_{\rm E}}{2\eta_0}\, t. \tag{7}$$

This is the classical Lucas-Washburn equation (1) with $h \sim t^{1/2}$ scaling.

We would like to point out some general requirements for systems to have the $t^{1/2}$ scaling. The left-hand side of the force balance equation (5) is a thermodynamic force, which can be derived from conserved potential energy. This term must not depend on h. A counterexample is the capillary rising when gravity is important. In this case, the gravitational force is proportional to the mass of the fluid, and $h(t)$ eventually approaches an asymptotic Jurin's height at long time. The right-hand side of the force balance equation (5) is related to the energy dissipation. In the simplest form of Eq. (4), the force is due to the viscous dissipation resulting from the parabolic flow profile. This term must be proportional to h. A counterexample is the dissipation in the meniscus at the fluid front. In this case, a friction force related to the meniscus has no h-dependency, and the resulting evolution of $h(t)$ would not be of the Lucas-Washburn type ($t^{1/2}$).

In the following, we will consider the imbibition of polymeric fluids into nanopores. We focus on the situation where the Lucas-Washburn scaling $t^{1/2}$ is valid, and consider various effects that may lead to different prefactors in a modified LWE.

2.1. Confinement effect

When the pore diameter is of the same order as the molecule size, as in our case of polymeric fluids, the conformation of the polymer chain is perturbed. In general, polymer chains have higher free energy in the pores than in the bulk. This reduces the driving force for the filling, and may be described by an effective surface tension

$$\gamma_{\text{eff}} = \gamma \cos\theta_{\text{E}} - \Delta f \frac{R}{2} \tag{8}$$

where Δf is the change in the free energy density of a polymer melt under confinement in comparison to the bulk.

We can evaluate Δf using the blob model [15]. The polymer chains are under biaxial confinement and can be viewed as a sequence of compression blobs of the pore diameter $2R$. For ideal chains, the number of monomer g in each compression blob is given by $g = (2R/b)^2$, where b is the statistical length of the monomer (Kuhn length). The number of blobs per chain is given by N/g, where N is the number of monomers per chain. The free energy penalty due to confinement is of the order of k_BT per compression blob, i.e., $\Delta F = k_BTN/g = k_BT\,Nb^2/(4R^2)$. To obtain the free energy density, we use the number density of the polymer chain $1/(\mathrm{v}_0 N)$, where v_0 is the monomer volume. The difference in the free energy density Δf is then given by

$$\Delta f = \frac{1}{\mathrm{v}_0 N} \times k_BT \frac{Nb^2}{4R^2} = k_BT \frac{b^2}{4\mathrm{v}_0 R^2}. \tag{9}$$

We estimate the effect of confinement by comparing the two terms in Eq. (8). The ratio between these two terms is

$$\frac{k_BT}{\gamma \cos\theta_{\text{E}}} \frac{b^2}{8\mathrm{v}_0 R}. \tag{10}$$

Using the experiments of PEO in AAO pores as an example [14]: $\mathrm{v}_0 = 6.04 \times 10^{-29}$ m^3, $T = 358$ K, $k_BT = 4.94 \times 10^{-21}$ J, $\gamma \cos\theta_{\text{E}} = 0.02$ J/m^2, $b = 0.68$ nm, and $2R = 35$ nm, this results a ratio of 0.014. This is too small an effect to account for the increase in the effective viscosity.

2.2. Dead zone effect

For simple fluids, the flow profile inside the pore has a parabolic profile, a result of the Stokes equation and no-slip boundary condition on the wall. For polymeric fluids, the polymer chains near the inner wall can be strongly adsorbed. There exists experimental evidences for that from dielectric spectroscopy measurements for polymers confined to nanoporous alumina [16]. These immobile chains create a "dead zone" of thickness ΔR. We define an effective radius of the pore by $R_{\rm eff} = R - \Delta R$, and consider the effect of dead zone on the imbibition speed.

Outside the dead zone, the polymer melts exhibit a macroscopic flow with the usual parabolic profile. We rewrite Eq. (6) in term of a pressure

$$v = \frac{R^2}{8\eta_0 h}\Delta P, \quad \Delta P = \frac{2\gamma\cos\theta_{\rm E}}{R}, \tag{11}$$

where ΔP is the Laplace pressure that drives the imbibition. This term remains unchanged when the dead zone is considered, but we have to replace R^2 in the numerator by $R_{\rm eff}^2$. Since only $R_{\rm eff}^2/R^2$ portion of the polymer contributes to the flow, the fluid front advances at the rate

$$\dot{h} = v\frac{R_{\rm eff}^2}{R^2} = \frac{R_{\rm eff}^4}{8\eta_0 h R^2}\Delta P = \frac{R_{\rm eff}^4}{8\eta_0 h R^2}\frac{2\gamma\cos\theta_{\rm E}}{R}. \tag{12}$$

Comparing the above equation to Eq. (6) with η_0 replaced by an effective viscosity $\eta_{\rm eff}$, defined by $\dot{h} = \gamma\cos\theta_{\rm E} R/(4\eta_{\rm eff} h)$, we obtain the following expression for $\eta_{\rm eff}$

$$\frac{\eta_{\rm eff}}{\eta_0} = \left(\frac{R}{R_{\rm eff}}\right)^4. \tag{13}$$

Since $R_{\rm eff} < R$, we have $\eta_{\rm eff} > \eta_0$. Also because of the fourth power, the effect of dead zone is quite substantial even for a small change in $R_{\rm eff}$. This is the origin of the slow-down in the imbibition dynamics for shorter chains.

2.3. Reptation under imbibition

As the pore radius is reduced and becomes comparable to the thickness of the dead zone, the macroscopic flow is nearly stopped. The material transport under very strong confinement is achieved mainly by the reptation of free polymer chains

in a network driven by the pressure gradient. Johner et al. has developed a theoretic framework for this scenario [8]. Here we present their results for completeness, while also include the pore-size dependence of the pressure gradient.

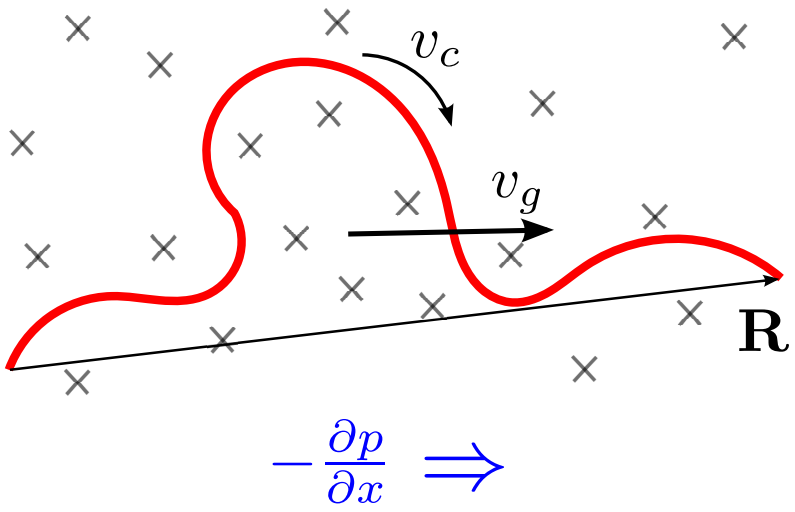

FIG. 2. Schematics of reptation motion of a polymer chain under a pressure gradient.

Figure 2 shows one single free chain under a pressure gradient. A polymer chain is constrained by other chains due to entanglements, and as such it can only move along the "reptation tube". Each free polymer chain experiences a driving force due to the pressure difference along the chain $[-p(x+R_x)+p(x)]\,\ell^2 = -\ell^2 R_x\,\partial p/\partial x$, where ℓ^2 is the cross section and R_x is the x-component of the end-to-end vector. The friction to the free chain is given by $N\zeta v_c$, where N is number of segments, ζ is the friction constant for one Kuhn segment, and v_c is the chain's velocity along the reptation tube. The balance between the pressure gradient and the frictional force gives

$$v_c = -\frac{\ell^2}{\zeta N} R_x \frac{\partial p}{\partial x}. \tag{14}$$

The averaged velocity for the center of mass of the polymer is

$$\langle v_g \rangle = \left\langle \frac{R_x}{L} v_c \right\rangle = -\frac{\ell^2}{\zeta N L} \langle R_x^2 \rangle \frac{\partial p}{\partial x} = -\frac{\ell^2 a_t}{3\zeta N} \frac{\partial p}{\partial x}, \tag{15}$$

where L is the contour length of the tube, given by $L = (N/N_e)a_t$. N_e is the entanglement length and $a_t = \sqrt{N_e} b$ is the tube diameter. The average of R_x^2 is assumed to be ideal $\langle R_x^2 \rangle = (1/3)Nb^2$.

If the fraction of polymer chains participating the reptation is φ, the filling speed is then given by

$$\dot{h} = \varphi \langle v_g \rangle = \varphi \frac{\ell^2 a_t}{3\zeta N} \frac{2\gamma \cos\theta_{\rm E}}{hR}, \tag{16}$$

where we averaged the pressure gradient along the whole fluid, $-\partial p/\partial x = \Delta P/h = 2\gamma \cos\theta_{\rm E}$.

Complication arises when one needs to specify the cross-section ℓ^2. One natural choice is the cross-section of the reptation tube,

$$\ell^2 = a_t^2 \quad \Rightarrow \quad \dot{h} = \varphi \frac{N_{\rm e}^{3/2} b^3}{3\zeta N} \frac{2\gamma \cos\theta_{\rm E}}{hR}. \tag{17}$$

In Ref. [8], Johner et al. used

$$\ell^2 = \frac{N_{\rm e} b^3}{\sqrt{N_{\rm e}} b} = N_{\rm e}^{1/2} b^2 \quad \Rightarrow \quad \dot{h} = \varphi \frac{N_{\rm e} b^3}{3\zeta N} \frac{2\gamma \cos\theta_{\rm E}}{hR}. \tag{18}$$

The only difference is in the scaling with respect to $N_{\rm e}$. Here we shall assume a general form of

$$\dot{h} = \varphi \frac{N_{\rm e}^{\alpha} b^3}{3\zeta N} \frac{2\gamma \cos\theta_{\rm E}}{hR}, \tag{19}$$

where α is the exponent.

2.4. Summary on effective viscosity

In the case of $R_g \ll R$, the dead-zone effect is dominant and the filling dynamics is given by Eq. (12). In the other limit, $R_g \gg R$, the reptation mode is important and the filling dynamics is governed by Eq. (19). A simple formula to interpolate these two limits is

$$\dot{h} = \left[\frac{R_{\rm eff}^4}{8\eta_0 R^2} + \varphi \frac{N_{\rm e}^{\alpha} b^3}{3\zeta N} \right] \frac{2\gamma \cos\theta_{\rm E}}{hR} \tag{20}$$

We again define an effective viscosity by

$$\dot{h} = \frac{\gamma \cos\theta_{\rm E} R}{4\eta_{\rm eff} h} = \frac{R^2}{8\eta_{\rm eff}} \frac{2\gamma \cos\theta_{\rm E}}{hR}. \tag{21}$$

Comparing the above two equations, we obtain

$$\frac{\eta_{\rm eff}}{\eta_0} = \left[\left(\frac{R_{\rm eff}}{R} \right)^4 + \varphi \frac{8 N_{\rm e}^{\alpha} b^3 \eta_0}{3\zeta N R^2} \right]^{-1}. \tag{22}$$

In the limit of small pore, the first term in the square bracket vanishes because $R_{\text{eff}} \to 0$. The effective viscosity is then dominant by the second term

$$\eta_{\text{eff}} \sim \eta_0 \left(\frac{\eta_0}{N}\right)^{-1} \sim N^1. \tag{23}$$

This is quite different than the bulk scaling $\eta_0 \sim N^3$. Thus confined polymers show an enhanced mobility, consistent with the experiment findings in Refs. [13] and [14] that have shown exponents of ~ 1.4 and ~ 0.9, respectively.

3. COMPARISON TO THE EXPERIMENT AND DISCUSSION

We compare our theoretical model with the capillary filling experiments in Ref. [14]. The bulk properties of PEO melts of different molecular weights are shown in Tab. I. A fit to the viscosity gives $\eta_0 \sim N^{2.91}$, which indicates that we may use the standard formulation of Doi-Edwards model [17]

$$\eta_0 \simeq \frac{\zeta b^2}{\mathrm{v}_0} \frac{N^3}{N_{\mathrm{e}}^2}. \tag{24}$$

Sample	γ ($^{-3}$ N/m)	θ_{e} (deg)	η_0 (Pa·s)
PEO 50k	29.1	44.0	4.3×10^2
PEO 100k	27.8	44.5	3.9×10^3
PEO 280k	28.0	44.0	1.5×10^5
PEO 500k	28.1	40.7	4.6×10^5
PEO 1M	28.0	47.7	2.7×10^6

TABLE I. PEO melt properties.

The effective viscosity (22) can be rewritten as

$$\frac{\eta_{\text{eff}}}{\eta_0} = \left[f(\Delta R, R) + g(\phi, N, R)\right]^{-1}. \tag{25}$$

The first function f is related to the dead-zone

$$f(\Delta R, R) = \begin{cases} (1 - \frac{\Delta R}{R})^4 & \text{if } R > \Delta R \\ 0 & \text{if } R < \Delta R \end{cases} \tag{26}$$

The second function g is from the reptation model,

$$g(\phi, N, R) = \varphi \frac{8N_e^{\alpha} b^3}{3\zeta} \frac{\eta_0}{NR^2} = \varphi \frac{8N_e^{\alpha-2} b^5}{3v_0} \frac{N^2}{R^2} = \phi \frac{N^2}{R^2}, \tag{27}$$

where we have used Eq. (24) and grouped parameters into one single factor ϕ. In the end, we have two free parameters: ΔR and ϕ. In principle, these two parameters may vary for different pore radii and molecular weights. As a first attempt, we neglect those dependence and assume ΔR and ϕ are constants.

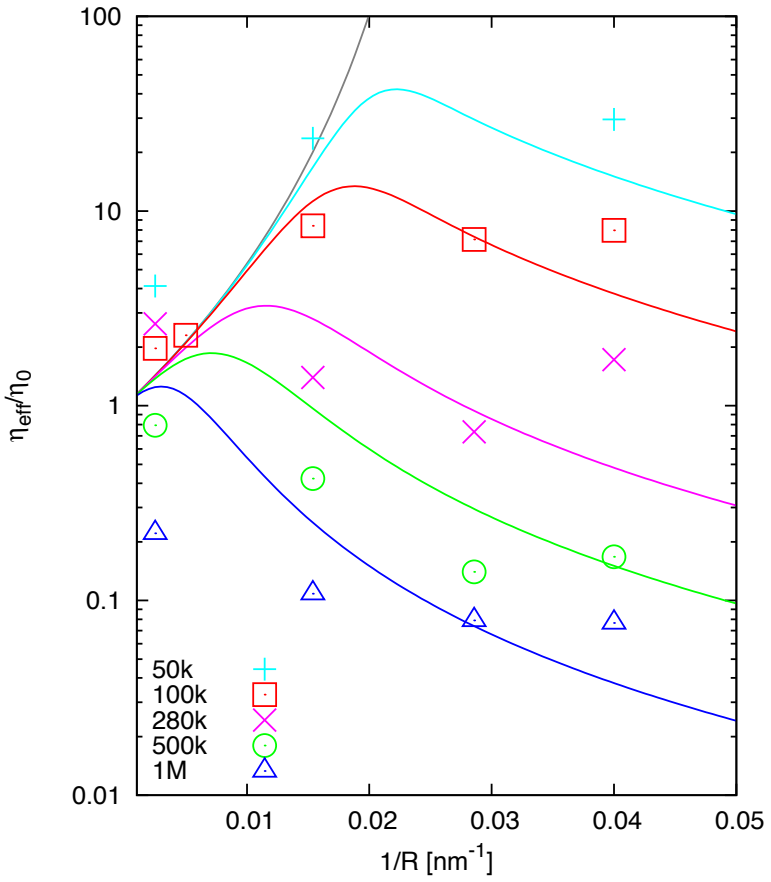

FIG. 3. Comparison between the experiment and theory. The symbols are shown for the experimental data taken from Ref. [14]. The lines are from theoretical prediction of Eq. (25).

Figure 3 shows the comparison between the experiment and theory. We plot the ratio of the effective viscosity to the bulk viscosity as a function of $1/R$, the inverse of the pore radius, for a polymer with various molecular weights. The fitting

parameters are obtained by global fitting resulting to:

$$\Delta R = 34.3\text{nm}, \quad \phi = 3.21 \times 10^{-5}\ [\text{nm}^2]. \tag{28}$$

The theoretic prediction is in qualitative agreement with the experimental data. Most importantly, the theory has captured the non-monotonic variation in the effective viscosity. The main reason for the non-monotonic behavior is that functions f and g vary differently with respect to $1/R$. In the large pore limit, these two functions $f \to 1$ while $g \to 0$, and the effective viscosity approaches the bulk value, $\eta_{\text{eff}} \to \eta_0$. As the pore radius decreases ($1/R$ increases), the effect of the dead zone becomes important and eventually stops the macroscopic flow. Accordingly, the function f decreases. On the other hand, for small pores the reptation motion of the entangled polymer becomes effective and function g increases. It is the opposite trends in the functions f and g that lead to the non-monotonic variation of the effective viscosity as observed experimentally.

The inversion point, i.e., the value of $1/R$ when the effective viscosity has its maximum, is a function of the molecular weight. For polymers of low molecular weight, the inversion point corresponds to a pore radius that is comparable with the thickness of the dead-zone, ΔR. Alternatively, for longer chains, the maximum shifts towards the $1/R \to 0$, i.e., to the very weak confinement limit.

4. SUMMARY

We present a theoretical model for the imbibition dynamics of entangled polymer melts into nanopores. Experiments have demonstrated the validity of the $t^{1/2}$ scaling, however the Lucas-Washburn equation breaks down because of the prefactor. We have considered various effects that can affect the imbibition dynamics while preserving the $t^{1/2}$ scaling: (i) The effect of confinement. Biaxial confinement of polymer chains induces a penalty in the free energy, but the effect is too small to explain the slow-down in dynamics. (ii) The effect of adsorption. Strongly-adsorbed chains create a dead zone, reducing the pore radius, and leading to an increase in the effective viscosity. (iii) The effect of reptation under a pressure gradient: The reptation of polymer chains under strong confinement [8] enhances the mobility

of confined chains, leading to faster imbibition. The overall imbibition dynamics can be discussed by the competition of the latter two mechanisms. The theoretical predictions captures the main features of the experiment being in a qualitative agreement with the experiments.

ACKNOWLEDGMENTS

This work in Beihang University was supported by the National Natural Science Foundation of China (NSFC) through the Grants No. 21504004 and No. 21774004. M.D. acknowledges the financial support of the Chinese Central Government via the Thousand Talents Program.

---

[1] R. Lucas, "Ueber das zeitgesetz des kapillaren aufstiegs von flüssigkeiten," Kolloid-Zeitschrift **23**, 15–22 (1918).

[2] Edward W. Washburn, "The dynamics of capillary flow," Phys. Rev. **17**, 273–283 (1921).

[3] Pierre-Gilles de Gennes, Françoise Brochard-Wyart, and David Quéré, *Capillarity and Wetting Phenomena* (Springer, 2004).

[4] Salim Ok, Martin Steinhart, Anca Şerbescu, Cornelius Franz, Fabián Vaca Chávez, and Kay Saalwächter, "Confinement effects on chain dynamics and local chain order in entangled polymer melts," Macromolecules **43**, 4429–4434 (2010).

[5] Fabien Chauvet, Sandrine Geoffroy, Abdelkrim Hamoumi, Marc Prat, and Pierre Joseph, "Roles of gas in capillary filling of nanoslits," Soft Matter **8**, 10738 (2012).

[6] Lena Mammen, Periklis Papadopoulos, Kathrin Friedemann, Stefanie Wanka, Daniel Crespy, Doris Vollmer, and Hans-Jürgen Butt, "Transparent and airtight silica nano- and microchannels with uniform tubular cross-section," Soft Matter **9**, 9824 (2013).

[7] Bing-Yang Cao, Min Yang, and Guo-Jie Hu, "Capillary filling dynamics of polymer melts in nanopores: experiments and rheological modelling," RSC Adv. **6**, 7553–7559 (2016).

[8] A. Johner, K. Shin, and S. Obukhov, "Nanofluidity of a polymer melt: Breakdown of Poiseuille's flow model," Europhys. Lett. **91**, 38002 (2010).

[9] Nam-Kyung Lee, Diddo Diddens, Hendrik Meyer, and Albert Johner, "Local chain segregation and entanglements in a confined polymer melt," Phys. Rev. Lett. **118**, 067802 (2017).

[10] D. I. Dimitrov, A. Milchev, and K. Binder, "Capillary rise in nanopores: Molecular dynamics evidence for the lucas-washburn equation," Phys. Rev. Lett. **99**, 054501 (2007).

[11] Mikhail R. Stukan, Patrice Ligneul, John P. Crawshaw, and Edo S. Boek, "Spontaneous imbibition in nanopores of different roughness and wettability," Langmuir **26**, 13342–13352 (2010).

[12] Wylie Stroberg, Sinan Keten, and Wing Kam Liu, "Hydrodynamics of capillary imbibition under nanoconfinement," Langmuir **28**, 14488–14495 (2012).

[13] Kyusoon Shin, Sergei Obukhov, Jiun-Tai Chen, June Huh, Yoontae Hwang, Soonchun Mok, Priyanka Dobriyal, Pappannan Thiyagarajan, and Thomas P. Russell, "Enhanced mobility of confined polymers," Nat. Mater. **6**, 961–965 (2007).

[14] Yang Yao, Stelios Alexandris, Franziska Henrich, Günter Auernhammer, Martin Steinhart, Hans-Jürgen Butt, and George Floudas, "Complex dynamics of capillary imbibition of poly(ethylene oxide) melts in nanoporous alumina," J. Chem. Phys. **146**, 203320 (2017).

[15] Michael Rubinstein and Ralph H. Colby, *Polymer Physics* (Oxford University Press, Oxford, 2003).

[16] Stelios Alexandris, Georgios Sakellariou, Martin Steinhart, and George Floudas, "Dynamics of unentangled cis-1, 4-polyisoprene confined to nanoporous alumina," Macromolecules **47**, 3895–3900 (2014).

[17] Masao Doi and S.F. Edwards, *The Theory of Polymer Dynamics* (Clarendon Press, Oxford, 1994).